Article

Phase Transition and Negative Thermal Expansion in a Guanidinium Magnesium-Hypophosphite Hybrid Perovskites

Hong-Qiang Gao, Wen-Juan Wei, Yu-Hui Tan, and Yun-Zhi Tang

Chem. Mater., **Just Accepted Manuscript** • DOI: 10.1021/acs.chemmater.0c01654 • Publication Date (Web): 27 Jul 2020

Phase Transition and Negative Thermal Expansion in a Guanidinium Magnesium-Hypophosphite Hybrid Perovskites

Hong-Qiang Gao†, Wen-Juan Wei*,†, Yu-Hui Tan† and Yun-Zhi Tang*,†

†Engineering Research Institute, Jiangxi University of Science and Technology, Ganzhou 341000, China

ABSTRACT: When the A- and X-sites in three-dimensional (3D) ABX_3-type organic-inorganic hybrid perovskites are occupied by organic molecules, rich features and functionalities are carried. Herein, we report a new hybrid organic-inorganic ABX_3-type guanidnium hypophosphite perovskite-like [Gua][$Mg(H_2POO)_3$] (Gua = guanidinium, $C(NH_2)_3^+$), where its A- and X-sites are Gua cation and hypophosphite (H_2POO^-) bridges, respectively, therefore displays ample exotic characters. Results show that it undergoes a second-order irreversible phase transition and exhibits significant negative thermal expansion (NTE, α_b(LT) = -7.7(7) and α_b(HT) = -20.5(1) MK^{-1}) effect along the *b*-axis. In addition, UV-vis absorption spectrum, and calculated band structure and density of states demonstrate that the Gua cations donate to the large direct bandgap. These results show that hypophosphite perovskites provide a hopeful platform for preparation of new functional materials.

■ INTRODUCTION

Recently, a novel family of 3D hypophosphite perovskites with the general formula [A]$M(H_2POO)_3$, where A is protonated amines ($AmineH^+$), M is divalent cations (M^{2+}), and H_2POO^- is the hypophosphite anion, in the class of organic-inorganic hybrid perovskites has been discovered. These compounds have been studied extensively and fundamentally for their structural diversity, phase transition, magnetic, and other properties,[1-3] due to the more flexible H_2POO^- bridges exist in the structure, which gives rise to additional symmetry-breaking elements in the form of classically forbidden Glazer tilts and columnar shifts.[2] In addition, A-site cation sits within the hypophosphorous cage exhibit the pronounced off-centering, which donates to the variety of unconventional tilts and shifts. This intriguing structure promoted broad interest in properties and phase transition mechanism in these compounds, despite there have hitherto reported the manganum (Mn^{2+}) hypophosphite frameworks templated by various amines.[1] As a continuation of the search for novel hypophosphite-base frameworks, herein we report the study of guanidinium magnesium-hypophosphite perovskite with the chemical formula of [Gua][$Mg(H_2POO)_3$]. Based on the Goldschmidt tolerance factor [4, 5] (α = 0.95) and the defined distortion factor[1] (δ = 0.5% and 0.6%) of [Gua][$Mg(H_2POO)_3$], where these two factors are greater and less than that of homologous Mn^{2+} hypophosphite perovskite [Gua][$Mn(H_2POO)_3$], thus we predicted this compound likely forms more stable perovskite structure and is significantly less distorted than [Gua][$Mn(H_2POO)_3$], while it is more distortion than the [Gua]$Mg(HCOO)_3$ (α = 0.99), due to the effect of building the framework with an even smaller and larger effective size of Mg^{2+} and H_2POO^- than Mn^{2+} and $HCOO^-$, respectively. Meanwhile, [Gua][$Mg(H_2POO)_3$] displays a second-order phase transition, which arises from the distortion of framework and Gua cations. Inconceivably, [Gua][$Mg(H_2POO)_3$] displays a significant negative thermal expansion (NTE) along the *b*-axis,[6-8] which is the first time to be reported in the 3D hypophosphite-based perovskites.

■ EXPERIMENTAL SECTION

Synthesis. All chemicals and solvents were of reagent grade and used as received. The compound [Gua]$Mg(H_2POO)_3$ was prepared by a slow diffusion method. Typically for: a aqueous hypophosphorous acid solution (0.646 mL, 6 mmol) with 1 mmol magnesium carbonate was placed in bath sonication, followed by magnetic stirring and heating at 50 °C. Then 1 mmol guanidine carbonate was then added and stirred. This solution was placed into vapour diffusion chambers with N,N-dimethylformamide (DMF). The sealed solutions were kept at room temperature until the colorless crystals have precipitated from liquid.

Powder X-ray diffraction. Powder X-ray diffraction (PXRD) patterns were collected at room temperature on a Empyrean (X'Pert PRO, PANalytical B.V.) apparatus with a Cu radiation (λ=1.5148Å, operating at 40 KV and 30 mA). The sample was prepared by full of grinding and diffraction data were collected in the range of 10 – 55° at a rate of 3°/min.

Variable-Temperature Single Crystal X-ray Diffraction. Single-crystal X-ray diffraction experiments were performed at a nitrogen stream condition using a Rigaku XtaLAB PRO MM007 HF diffractometer with Pilatus 200 k Silicon Diaray Detector. The crystals were glued on a glass fiber for measurement. Data were collected using Cu-Kα radiation (λ = 1.54184 Å) by the ω scan approach at a temperature in the range of 200~280 K at the interval of 20 K, and 280~320 K at the interval of 10 K and then 320~360 K at the interval of 20 K, respectively. Data collection, cell determination and refinement and

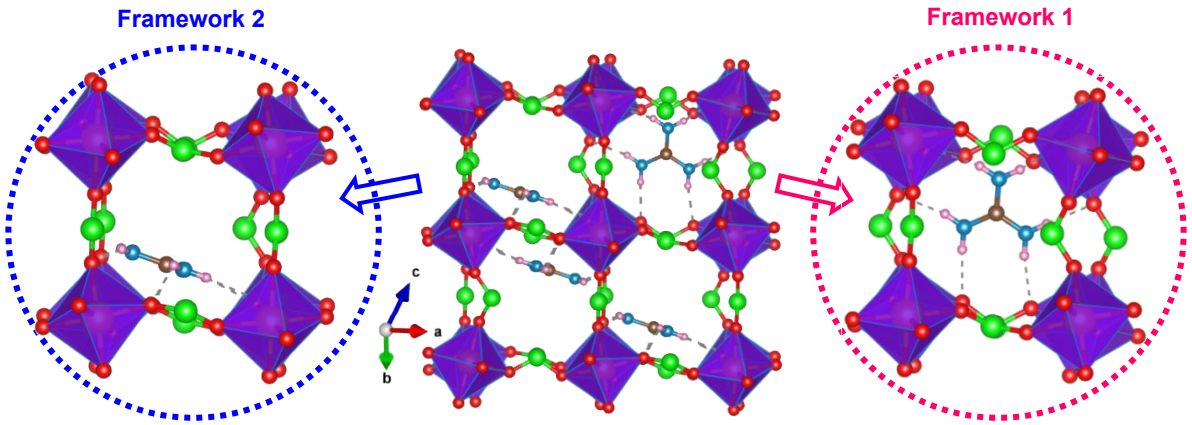

Figure 1. The crystal structure of [Gua]Mg(H_2POO)$_3$ at 290 K. Colour: Mg, orange; P, viridis; O, red; C, aubergine; N, cyan; H, pink. The gray dotted lines represent hydrogen bonds. The figures in the two virtual boxes represent amplified two modes frameworks of 1 and 2, respectively.

data reduction were applied with *CrysAlis*^{Pro} program. The structures were solved and refined using the direct method and full matrix least-squares procedure on F^2 by the SHELXS and SHELXL 97 programs.[9] All non-hydrogen atoms with anisotropic thermal parameters were refined and all hydrogen atoms were located from the electron density map and refined using a riding mode and isotropic displacement parameters constrained to 1.2 times those of their adjacent carbon or oxygen atoms. These data can be found on the Cambridge Crystallographic Data Centre at liberty via www.ccdc.cam.ac.uk/data_request/cif. CCDC Nos. 2006706-2006716.

Heat Capacity. Heat capacity was measured using a PPMS DynaCool Cryogen-free System (Physical Property Measurement System® DynaCool™, Quantum Design, USA) equipped with a VSM module up to $\mu_0 H$ = 5 T. Nitrogen was used as a purging gas. The excess heat capacity values associated with the phase transitions were evaluated by subtraction from the data the baselines representing variations in the absence of the phase transitions.

Dielectric Properties. The dielectric measurements were carried out with powder samples in the form of tablet which used as electrodes by pasting silver conduction on its both surfaces compactly. The dielectric constants of the compounds were confirmed with an Agilent or a Model TH2828A impedance analyzer over the frequency range from 500 Hz to 1 MHz in the process of heating and then cooling.

DSC. At ambient pressure, the thermal properties of [Gua]Mg(H_2POO)$_3$ were measured using differential scanning calorimetry (DSC) with a TA Q2000 DSC instrument. The heating and cooling rates of the powdered sample were recorded at intervals of about 10 K/min. Indium standard was used for the temperature and enthalpy calibration.

Density Functional Theory Calculations. The DFT calculations of the band structure and density of states (DOS) have been performed using the CASTEP code,[10] a total energy package based on pseudopotentail density functional theory (DFT).[11, 12] The correlation and exchange terms in the Hamiltonian were described by the functionals developped by Perdew, Burke and Ernzerhof (PBE)[13] in the generalized gradient approximation (GGA)[14] form. Optimized ultrasoft pseudopotentials were adopted. The energy cutoff was set to 400 eV, and a 6 × 4 × 4 Monkhorst–Pack grid of *k*-points was used.

■ RESULTS

Structural Analysis. The crystal structure of [Gua]Mg(H_2POO)$_3$ at 290 K (Figure 1) crystalizes in a triclinic space group $P\bar{1}$ with cell parameters of a = 8.98497(10), b = 9.07444(7) and c = 15.61097(16) Å, V = 1061.45(2) Å^3, as described in Table S1, which all significantly larger than the parameters in the congeneric perovskite [Gua]Mg($HCOO$)$_3$ due to H_2POO^- (4.75Å) has a larger effective size than $HCOO^-$ (4.47Å).[1] This structure forms a conventional 3D ABX_3 perovskite framework,[15-17] where A, B and X are Gua, Mg^{2+} and H_2POO^-, respectively, with fully ordered Gua cations located far from the center of the [Mg(H_2POO)$_3$]$^-$ framework cavities. Each distorted MgO_6 octahedron is linked to six neighbouring octahedrons via H_2POO^- ligands with smaller distortion O-P-O angles in the range of 115.3(1)-118.3(1)° than the O-C-O angles of 126.9(4) and 129.0(2)° in the isomorphic [Gua]Mg($HCOO$)$_3$ perovskite,[18] which indicates the former has a greater degree of distortion than the latter. Where the Mg-O bond lengths are in the range of 2.0372(28)–2.1394(12) Å and the *cis* O-Mg-O angles are in the range of 84.39(7)–101.88(7)° while the *trans* O–Mg–O angles lie in the range of 170.93(7)–177.62(7)°. Gua cations order parallel to two perpendicular planes and thus form two kinds of frameworks of 1 and 2 (Figure 1 'right' and 'left'). Meanwhile, all six N–H bonds from the each Gua cation hydrogen-bonded to the [Mg(H_2POO)$_3$]$^-$ framework by six hydrogen bonds N–H···O with N···O distances in the range of 2.8687(24)~3.1177(35) Å and the corresponding N-H···O angles in the range of 170.0(4)~167.5(4)° in framework 1 (Figures 1 'right' and S3a, Table S2), and N···O distances in the range of 2.9073(33)~3.1151(40) Å and the corresponding N-H···O angles in the range of 170.0(4)~167.5(4)° in framework 2 (Figures 1 'left' and S3b, Table S2), respectively. Hence, H-bonding appears to drive the structural distortion and

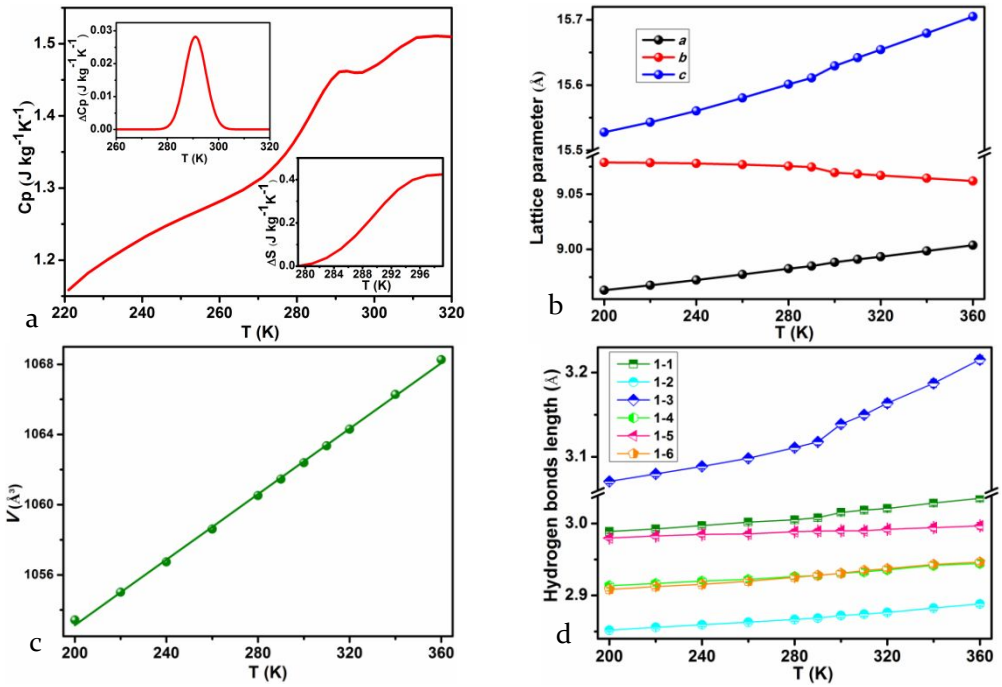

Figure 2. (a) The heat capacity of $[Gua]Mg(H_2POO)_3$ measured in a heating mode. The insets show the change in ΔC_p and ΔS related to the phase transition. Temperature dependence of lattice parameters (b), cell volume (c) and hydrogen bonds lengths (d).

Gua cation off-centering. The synergistic effect of Gua cations and frameworks enables the entire structure have an $a^-b^-c^-$ Glazer tilt system according to the Glazer notation (Figure S2).[1, 19-21]

Thermal Analysis. Just as conventional formate perovskite families $[AmineH^+][M(HCOO)_3]$ ($AmineH^+$ = organic amine cations, M^{2+} = divalent metal cations), as building blocks for luminescence, ferroelectric, magnetic and multiferroic properties, undergo temperature induced structural phase transitions associated with ordering of the organic cations and distortion of the metal frameworks.[22-24] We hypothesized that this congeneric perovskite $[Gua]Mg(H_2POO)_3$ also would responds to temperature-induced phase transition, therefore, we investigate its thermodynamic behavior by differential scanning calorimeter (DSC) measurement. The result indicates that a small bulge appeared at 291 K during heating and disappeared during cooling (Figure S4), which suggests that $[Gua]Mg(H_2POO)_3$ shows a 2nd-order irreversible phase transition, just like in the $[Gua]Mn(H_2POO)_3$. Further heat capacity (C_p) measurement displays a small feature at the 291 K upon cooling process (Figure 2a). By fitting the C_p data to probe the excess heat capacity ΔC_p, and then integrate the $\Delta C_p/T$ curve to yield a value of entropy ΔS for phase transition of 0.42 J $kg^{-1}K^{-1}$ (0.24 J $mol^{-1}K^{-1}$) (Figure 2a 'insert'), this value is consistent with a 2nd-order phase transition.

Variable Temperature Single Crystal X-ray Diffraction Analysis. To further verify the presence of phase transition, we test the variable temperauture single crystal X-ray diffractions in the range of 200~360 K, results exhibit a triclinic $P\bar{1}$ to triclinic $P\bar{1}$ phase transition for $[Gua]Mg(H_2POO)_3$ between two phases accompanied by a small inflection point on cell parameters *b* and *c* between 290 and 300 K (Figure 2b). Here we define the phase below 291 K as the low-temperature (LT) phase, and the phase above 291 K as the high-temperature (HT) phase. As a result, *a*- and *c*-axes show positive thermal expansion (PTE) with thermal expansion coefficients α_a(LT) = 31.1(5) and α_a(HT) = 30.4(2) MK^{-1}, and α_c(LT) = 61.8(2) and α_c(HT) = 82.3(1) MK^{-1}, respectively, while *b*-axis presents a negative thermal expansion (NTE) with thermal expansion coefficients α_b(LT) = -7.7(7) and α_b(HT) = -20.5(1) MK^{-1}, with increasing temperature (Table S3).[25] These NTE coefficients have the similar magnitude of those from the perovskite-like metal-organic frameworks, $[C(NH_2)_3][M(HCOO)_3]$ (M = Mn, Fe, Co and Zn), but an order of magnitude lower than those from $[C(NH_2)_3][Cd(HCOO)_3]$.[7] Nevertheless, cell volume (*V*) displays fine linear expansion accompanied by thermal expansion coefficient of α_V = 88.6(1.1) MK^{-1} with rising temperature (Figure 2c), which corresponds to the 2nd-order phase transition to be consistent with the thermal results. Meanwhile, hydrogen bonds in frameworks 1 and 2 show a normal trend, which all increase upon heating except N-H···O (1-3) in framework 1 and N-H···O (2-6) in framework 2 expand from 3.1177(35) to 3.1389(35) Å and from 3.1151(40) to 3.1218(47) Å, respectively, with a large elongation magnitude of 0.68% and 0.22% between 290 and 300 K, which results in overall weakening of the hydrogen-bonding when increasing temperature (Figures 2d and S5a).

In order to understand the mechanism of NTE behavior of $[Gua]Mg(H_2POO)_3$, we simplified the framework as a 'hinge-strut' like architecture,[6, 26, 27] which is a prototypical structural motif responsible for anisotropic thermal expansion in framework materials. In this simplified model, the H_2POO^- ligand and Mg^{2+} cation represent the

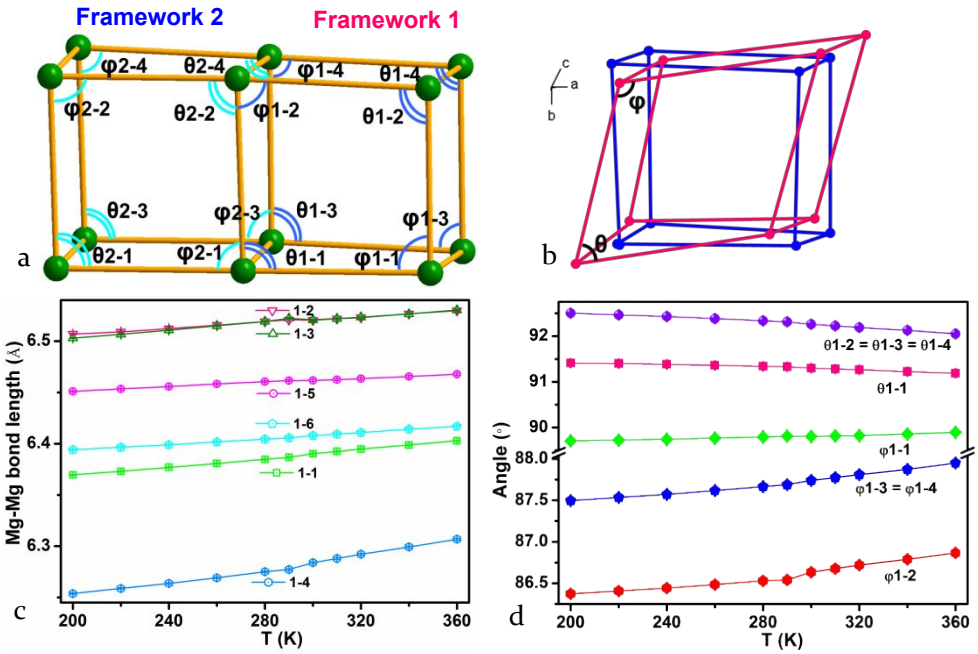

Figure 3. (a) The "hinge-strut" like structure models for frameworks 1 and 2. (b) Demonstrate the "hinge-strut" model of at low (blue) and high (peach) temperature. (c) Temperature-dependence of Mg-Mg bonds in the framework 1. (d) Temperature-dependence of hinge angles θ and φ in the frameworks 1 and 2.

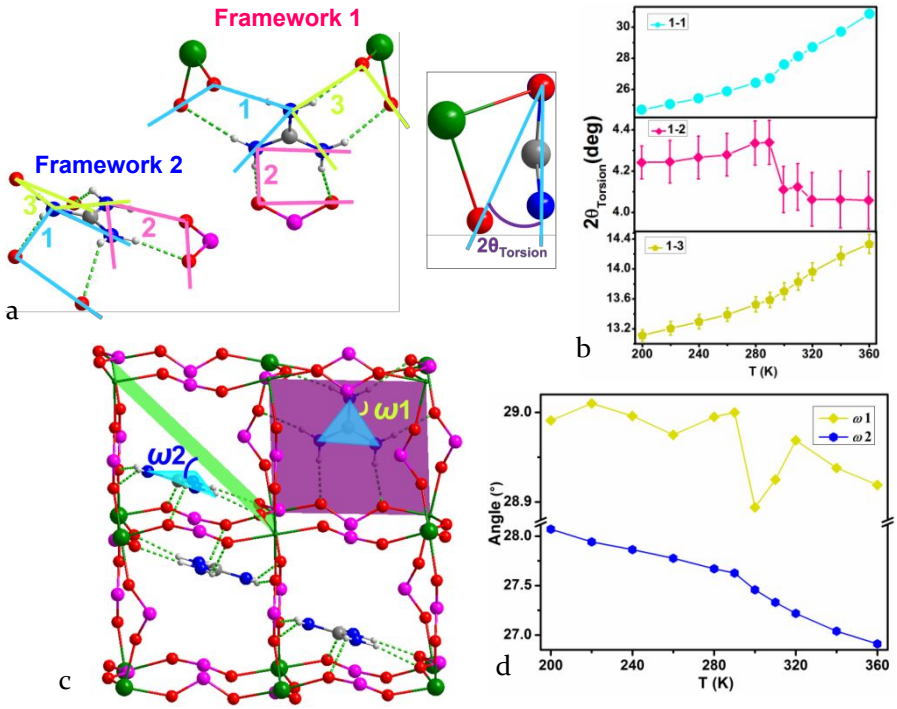

Figure 4. (a) Schematic diagrams of $2\theta_{Torsion}$ in frameworks 1 and 2, respectively. (b) Evolution diagram of $2\theta_{Torsion}$ with temperature change in framework 1. (c-d) The dihedral angles (ω1 and ω2) between Gua cation planes and body diagonal planes of the framework represent the tilting of Gua cations as a function of temperature.

hinge and strut, respectively, and the hinge angles are denoted as θ and φ (Figures 3a and b). Upon heating from 200 to 360 K, the lengths of Mg-O bonds and Mg-Mg bonds increase gradually (Figures 3c and S5b, Tables S4 and S6), meanwhile, hydrogen bonds between the Gua cations and frameworks in the frameworks 1 and 2 are overall weakened when increasing temperature (Figures 2d and S5a). These cooperative structural variations lead to an increased degree of freedom for structure to move, resulting the distortion of the MgO_6 octahedron and twist of the H_2POO^- ligands, thereby inducing the significant variation in the 'hinge-strut' model accompanied by an increase in average φ by 0.49% and an decrease in average θ by 0.45% near phase transition temperature (Figures 3d and S6a, Table S6). Such alterations give rise to a NTE along *b*-axis coupled to the large PTE along *a*- and *c*-axes.

In addition to the contribution from the $[Mg(H_2POO)_3]^-$ framework, Gua cations are also involved. The distortion of Gua cation is reflected by $2\theta_{Torsion}$(∠N-N-O-O) caused by the interaction between host framework and guest molecule.[28,29] As shown in Figure 4, six symmetrically inequivalent $2\theta_{Torsion}$ in frameworks 1 and 2, respectively, indicate both frameworks have different distortion trends (increasing of 3.30, -5.26 and 0.87% for framework 1 (Figure 4b and Table S7), and -0.13, -4.58 and 1.80% for framework 2 (Figure S6b and Table S7) between 290 and 300 K) with increasing of temperature, which in turn affects the deflection of Gua cations. In addition, the dihedral angles (ω1 and ω2) between Gua cation planes and body diagonal planes of the framework represent the tilting of Gua cations as a function of temperature. As shown in Figures 4c-d, ω1 displays an irregular pulsation as the temperature rises, while ω2 decreases regularly, where ω1 decreases from 29.0 to 28.9°, and ω2 decreases from 27.6 to 27.5° between 290 and 300 K, which indicates Gua cations oscillate randomly in framework 1 while they regularly rotate toward the body diagonal plane in framework 2 with increasing temperature.

Dielectric Analysis. It well known that dielectric permittivity ε is sensitive to local structural rearrangements, therefore it is a simple and effective avenue to investigate the phase transition and dynamic behaviors of structures.[30-35] The temperature-dependent dielectric responses of $[Gua]Mg(H_2POO)_3$ were measured on powder-pressed pellets at frequency ranges of 500 Hz~1 MHz. As shown in Figure 5 and S7, the real parts (ε') of dielectric constants reveal clear frequency-dependent responses. A dielectric anomaly at 291 K is observed upon heating at all frequencies, but the dielectric peaks are smoothed during cooling, which is consistent with the DSC result. The maximum peak value at 500 Hz is 367.7 a.u., while this value decreases by twenty times when frequency increases to 1 MHz during heating.

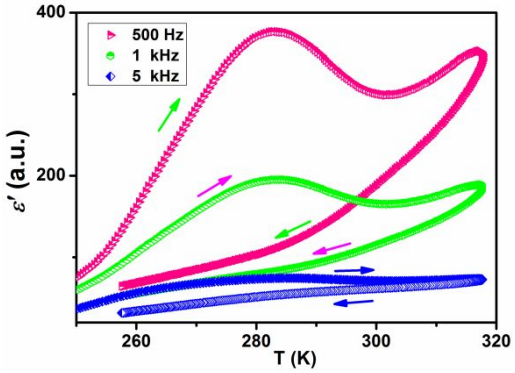

Figure 5. Temperature-variable the real parts (ε') of dielectric constants in the frequencies range from 500 Hz to 5 kHz of $[Gua]Mg(H_2POO)_3$ during heating and cooling processes.

UV-vis Absorption and Density Function Theory (DFT) Calculations. The UV-vis absorption spectrum of $[Gua]Mg(H_2POO)_3$ indicates a steep absorption edge at deep ultraviolet about 200 nm, which is consistent with that reported in some metal-formate perovskites $[C(NH_2)_3][M^{II}(HCOO)_3]$ (M=Mn, Fe, Co, Ni, Cu, and Zn).[36] The bandgap (E_g) is estimated to be about 5.94 eV by fitting above curve with *Tauc* equation[37] (Figure 6a), which is far exceeds that observed in the two direct band gap materials $(Gua)_2MI_4$ (M = Sn, Pb), for M = Sn, the band gap is specified as a relatively sharp absorption edge with a value of 2.06 eV; For M = Pb, the situation is more complex, as beside the band to band transition also an excitonic absorption is observed, a lower energy peak at 2.40 eV is assigned to the excitonic absorption and the higher energy one at 2.49 eV to the band gap of the material, which proves that determining the band gap from *Tauc* plots is critical in the presence of excitons.[38, 39]

In order to understand the electronic origin of bandgap, the band structures and energy gap of $[Gua]Mg(H_2POO)_3$ were calculated based on density functional theory (DFT) calculations.[11, 12] As shown in Figure 6b, $[Gua]Mg(H_2POO)_3$ shows a direct band gap at the Brillouin zones Γ point with energy value of 5.14 eV, which is slightly lower than the experimental value, this difference between experimental and calculated values may be due to the known generalized gradient approximation (GGA) functional underestimates the band gap.[40] Furthermore, the projected partial density of states (PDOS) plot shows that the states between C-2s2p and N-2s2p and between P-3s3p and O-2s2p overlap almost completely except for a peak near Fermi level, and H-1s state overlaps almost completely with the C-2p, N-2p and P-3p states. It indicates the strong covalent interactions in C-H, N-H and P-H bonds in the structure. Moreover, the valence band maximum of $[Gua]Mg(H_2POO)_3$ dominated by a lot of N-2p, O-2p orbitals and a bit of H-1s orbital, while the a mass of N-2p and P-3p orbitals and a small quantity of C-2p, P-3s and H-1s orbitals account for the conduction band minimum, meanwhile the Mg has almost no contribution, which indicates that the Gua cation and total framework are responsible for the band gap of $[Gua]Mg(H_2POO)_3$ (Figures 6c and S8).

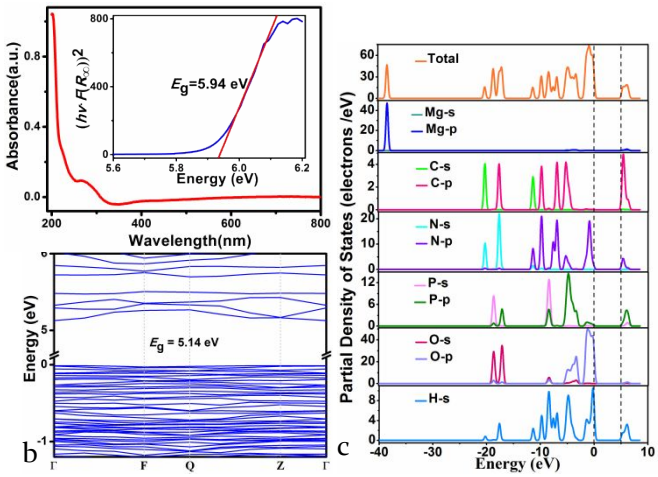

Figure 6. (a) UV-via absorption spectra of $[Gua]Mg(H_2POO)_3$. The inset shows the *Tauc* plot for $[Gua]Mg(H_2POO)_3$. (b) The calculated energy band structure of $[Gua]Mg(H_2POO)_3$. (c) Partial density of states (PDOS) for $[Gua]Mg(H_2POO)_3$.

■ CONCLUSION

In summary, we report a new hybrid organic-inorganic guanidnium hypophosphite perovskite $[C(NH_2)_3][Mg(H_2POO)_3]$, which crystallizes in the ABX_3-type perovskite-like triclinic structure. Using the single-crystal diffraction, thermal, and dielectric measurements demonstrate that this compound undergoes a second-order irreversible phase transition from a triclinic ($P\bar{1}$) to triclinic ($P\bar{1}$) at about 291 K. Variable-Temperature (VT) X-ray diffraction data reveals that this hypophosphite perovskite exhibits significant negative thermal expansion (NTE, α_b(LT) = -7.7(7) and α_b(HT) = -20.5(1) MK^{-1}) effect over the temperature range 200-360 K. In addition, the calculated band structure and density of states demonstrate that the guanidnium cations donate to the large direct bandgap.

■ ASSOCIATED CONTENT

Supporting Information.

The Supporting Information is available free of charge via the Internet at http://pubs.acs.org.

Figures S1-6: the unit, PXRD of $[Gua]Mg(H_2POO)_3$ at room temperature; octahedral layer tilts of $[Gua][Mg(H_2POO)_3]$ viewed normal to the three pseudo-cubic perovskite axes; the hydrogen bonds in the frameworks 1 and 2; DSC traces; temperature dependence of hydrogen bonds, Mg-Mg bonds lengths, $2\theta_{Torsion}$ and hinge angles θ and φ in the framework 2; Octahedral layer tilts of $[Gua]Mg(H_2POO)_3$ viewed normal to the three pseudo-cubic perovskite axes. decomposed DOS of *s*- and *p*-orbitals for $[Gua]Mg(H_2POO)_3$.

Tables S1-7: crystallographic data, hydrogen bonds lengths, the anisotropic coefficients of thermal expansion, the Mg···O bond lengths, Mg···Mg bond lengths, hinge angles, torsion angles in frameworks 1 and 2 of $[Gua]Mg(H_2POO)_3$ at different temperatures.

AUTHOR INFORMATION

Corresponding Author

*E-mail: wwenjuan20@163.com (W. W. J.).
*E-mail: tangyunzhi75@163.com (T. Y. Z.).

Notes

The authors declare no competing financial interest.

ACKNOWLEDGMENT

The authors acknowledge funding support from the National Natural Science Foundation of China (Grant Nos. 21761013 and 21671086) and the Education department of Jiangxi province (No. 204201400631) and the Fundamental Research Funds for the Central Universities (Jiangxi University of Science and Technology, No. 3401223417).

REFERENCES

(1) Wu, Y.; Shaker, S.; Brivio, F.; Murugavel, R.; Bristowe, P. D.; Cheetham, A. K. [Am]Mn$(H_2POO)_3$: A New Family of Hybrid Perovskites Based on the Hypophosphite Ligand. *J. Am. Chem. Soc.* **2017,** *139*, 16999-17002.

(2) Wu, Y.; Binford, T.; Hill, J. A.; Shaker, S.; Wang, J.; Cheetham, A. K. Hypophosphite hybrid perovskites: a platform for unconventional tilts and shifts. *Chem. Commun.* **2018,** *54*, 3751-3754.

(3) Wu, Y.; Halat, D. M.; Wei, F.; Binford, T.; Seymour, I. D.; Gaultois, M. W.; Shaker, S.; Wang, J.; Grey, C. P.; Cheetham, A. K. Mixed X-Site Formate-Hypophosphite Hybrid Perovskites. *Chemistry* **2018,** *24*, 11309-11313.

(4) Kieslich, G.; Sun, S.; Cheetham, A. K. An extended Tolerance Factor approach for organic-inorganic perovskites. *Chem. Sci.* **2015,** *6*, 3430-3433.

(5) Burger, S.; Ehrenreich, M. G.; Kieslich, G. Tolerance factors of hybrid organic–inorganic perovskites: recent improvements and current state of research. *J. Mater. Chem. A* **2018,** *6*, 21785-21793.

(6) Ogborn, J. M.; Collings, I. E.; Moggach, S. A.; Thompson, A. L.; Goodwin, A. L. Supramolecular mechanics in a metal–organic framework. *Chem. Sci.* **2012,** *3*, 3011.

(7) Collings, I. E.; Hill, J. A.; Cairns, A. B.; Cooper, R. I.; Thompson, A. L.; Parker, J. E.; Tang, C. C.; Goodwin, A. L. Compositional dependence of anomalous thermal expansion in perovskite-like ABX_3 formates. *Dalton Trans.* **2016,** *45*, 4169-78.

(8) Gao, H.; Wei, W.; Li, Y.; Wu, R.; Feng, G.; Li, W. Uniaxial Negative Thermal Expansion and Mechanical Properties of a Zinc-Formate Framework. *Materials* **2017,** *10*, 151.

(9) Dolomanov, O. V.; Bourhis, L. J.; Gildea, R. J.; Howard, J. A. K.; Puschmann, H. OLEX2: a complete structure solution, refinement and analysis program. *J. Appl. Crystallogr.* **2009,** *42*, 339-341.

(10) Clark, S. J.; Segall, M. D.; Pickard, C. J.; Hasnip, P. J.; Probert, M. I. J.; Refson, K.; Payne, M. C. First principles methods using CASTEP. *Z. Krist.-Cryst. Mater.* **2005,** *220*, 567-570.

(11) Kohn, W.; Sham, L. J. Self-Consistent Equations Including Exchange and Correlation Effects. *Phys. Rev.* **1965,** *140*, A1133-A1138.

(12) Payne, M. C.; Teter, M. P.; Allan, D. C.; Arias, T.; Joannopoulos, a. J. Iterative minimization techniques for ab initio total-energy calculations: molecular dynamics and conjugate gradients. *Rev. Mod. Phys.* **1992,** *64*, 1045.

(13) Perdew, J. P.; Burke, K.; Ernzerhof, M. Generalized gradient approximation made simple. *Phys. Rev. Lett.* **1996,** *77*, 3865.

(14) Perdew, J. P.; Wang, Y. Pair-distribution function and its coupling-constant average for the spin-polarized electron gas. *Phys. Rev. B Condens. Matter.* **1992,** *46*, 12947-12954.

(15) Pan, Q.; Liu, Z.-B.; Tang, Y.-Y.; Li, P.-F.; Ma, R.-W.; Wei, R.-Y.; Zhang, Y.; You, Y.-M.; Ye, H.-Y.; Xiong, R.-G. A Three-Dimensional Molecular Perovskite Ferroelectric: (3-Ammoniopyrrolidinium)$RbBr_3$. *J. Am. Chem. Soc.* **2017,** *139*, 3954–3957.

(16) Zhang, W.-Y.; Tang, Y.-Y.; Li, P.-F.; Shi, P.-P.; Liao, W.-Q.; Fu, D.-W.; Ye, H.-Y.; Zhang, Y.; Xiong, R.-G. Precise Molecular Design of High-T_c 3D Organic-Inorganic Perovskite Ferroelectric: [MeHdabco]RbI_3 (MeHdabco = N-Methyl-1,4-diazoniabicyclo[2.2.2]octane). *J. Am. Chem. Soc.* **2017,** *139*, 10897-10902.

(17) Zhang, H.-Y.; Song, X.-J.; Cheng, H.; Zeng, Y.-L.; Zhang, Y.; Li, P.-F.; Liao, W.-Q.; Xiong, R.-G. A Three-Dimensional Lead Halide Perovskite-Related Ferroelectric. *J. Am. Chem. Soc.* **2020,** *142*, 4604–4608.

(18) Rossin, A.; Chierotti, M. R.; Giambastiani, G.; Gobetto, R.; Peruzzini, M. Amine-templated polymeric Mg formates:

crystalline scaffolds exhibiting extensive hydrogen bonding. *CrystEngComm* **2012,** *14*, 4454.
(19) Glazer, A. M. The classification of tilted octahedra in perovskites. *Acta Cryst.* **1972,** *28*, 3384-3392.
(20) Glazer, A. M. Simple ways of determining perovskite structures. *Acta Cryst.* **1975,** *31*, 756-762.
(21) Howard, C. J.; Stokes, H. T. Group-Theoretical Analysis of Octahedral Tilting in Perovskites. *Acta Cryst.* **1998,** *B54*, 782-789.
(22) Xu, G. C.; Zhang, W.; Ma, X. M.; Chen, Y. H.; Zhang, L.; Cai, H. L.; Wang, Z. M.; Xiong, R. G.; Gao, S. Coexistence of magnetic and electric orderings in the metal-formate frameworks of $[NH_4][M(HCOO)_3]$. *J. Am. Chem. Soc.* **2011,** *133*, 14948-14951.
(23) Xu, G.-C.; Ma, X.-M.; Zhang, L.; Wang, Z.-M.; Gao, S. Disorder–order ferroelectric transition in the metal formate framework of $[NH_4][Zn(HCOO)_3]$. *J. Am. Chem. Soc.* **2010,** *132*, 9588-9590.
(24) Wang, Z.; Zhang, B.; Otsuka, T.; Inoue, K.; Kobayashi, H.; Kurmoo, M. Anionic NaCl-type frameworks of $[Mn^{II}(HCOO)_3^-]$, templated by alkylammonium, exhibit weak ferromagnetism. *Dalton Trans.* **2004,** *15*, 2209-2216.
(25) Cliffe, M. J.; Goodwin, A. L. PASCal: a principal axis strain calculator for thermal expansion and compressibility determination. *J. Appl. Crystallogr.* **2012,** *45*, 1321-1329.
(26) Goodwin, A. L.; Keen, D. A.; Tucker, M. G. Large negative linear compressibility of $Ag_3[Co(CN)_6]$. *Proc. Natl. Acad. Sci.* **2008,** *105*, 18708-18713.
(27) DeVries, L. D.; Barron, P. M.; Hurley, E. P.; Hu, C.; Choe, W. "Nanoscale lattice fence" in a metal-organic framework: interplay between hinged topology and highly anisotropic thermal response. *J. Am. Chem. Soc.* **2011,** *133*, 14848-14851.
(28) Viswanathan, M. Structural Tunability Controlled by Uniaxial Strength in a Hybrid Perovskite. *J. Phys. Chem. C* **2019,** *123*, 6711-6716.
(29) Wei, W.-J.; Li, C.; Li, L.-S.; Tang, Y. Z.; Jiang, X.-X.; Lin, Z. Phase transition, optical and dielectric properties regulated by anion-substitution in a homologous series of 2D hybrid organic-inorganic perovskites. *J. Mater. Chem. C* **2019,** *7*, 11964-11971.
(30) Shang, R.; Wang, Z.-M.; Gao, S. A 36-Fold Multiple Unit Cell and Switchable Anisotropic Dielectric Responses in an Ammonium Magnesium Formate Framework. *Angew. Chem. Int. Ed.* **2015,** *54*, 2534-2537.
(31) Li, C.; Li, L. S.; Wei, W. J.; Tan, Y. H. A Temperatural Semi-Memorized Phase Transition in a 1D Organic-Inorganic Hybrid Material of $Sb^{(III)}$-Based $[(CH_2)_3NH_2S]_2SbCl_5$. *Inorg. Chem.* **2019,** *58*, 9733-9737.
(32) You, Y. M.; Liao, W. Q.; Zhao, D.; Ye, H. Y.; Zhang, Y.; Zhou, Q.; Niu, X.; Wang, J.; Li, P. F.; Fu, D. W.; Wang, Z.; Gao, S.; Yang, K.; Liu, J. M.; Li, J.; Yan, Y.; Xiong, R. G. An organic-inorganic perovskite ferroelectric with large piezoelectric response. *Science* **2017,** *357*, 306-309.
(33) Ye, H. Y.; Tang, Y. Y.; Li, P. F.; Liao, W. Q.; Gao, J. X.; Hua, X. N.; Cai, H.; Shi, P. P.; You, Y. M.; Xiong, R. G. Metal-free three-dimensional perovskite ferroelectrics. *Science* **2018,** *361*, 151-155.
(34) Liao, W. Q.; Zhao, D.; Tang, Y. Y.; Zhang, Y.; Li, P. F.; Shi, P. P.; Chen, X. G.; You, Y. M.; Xiong, R. G. A molecular perovskite solid solution with piezoelectricity stronger than lead zirconate titanate. *Science* **2019,** *363*, 1206-1210.
(35) Gao, J.-X.; Zhang, W.-Y.; Wu, Z.-G.; Zheng, Y.-X.; Fu, D.-W. Enantiomorphic Perovskite Ferroelectrics with Circularly Polarized Luminescence. *J. Am. Chem. Soc.* **2020,** *142*, 4756–4761.
(36) Hu, K.-L.; Kurmoo, M.; Wang, Z.; Gao, S. Metal-Organic Perovskites: Synthesis, Structures, and Magnetic Properties of $[C(NH_2)_3][MII(HCOO)_3]$ (M=Mn, Fe, Co, Ni, Cu, and Zn; $C(NH_2)_3$= Guanidinium). *Chem. Eur. J.* **2009,** *15*, 12050–12064.
(37) Tauc, J. Absorption edge and internal electric fields in amorphous semiconductors. *Mater. Res. Bull.* **1970,** *5*, 721-729.
(38) Daub, M.; Haber, C.; Hillebrecht, H. Synthesis, Crystal Structures, Optical Properties, and Phase Transitions of the Layered Guanidinium-Based Hybrid Perovskites $[C(NH_2)_3]_2MI_4$; M= Sn, Pb. *Eur. J. Inorg. Chem*. **2017,** *2017*, 1120–1126.
(39) Green, M. A.; Jiang, Y.; Soufiani, A. M.; Ho-Baillie, A. Optical properties of photovoltaic organic-inorganic lead halide perovskites. *J. Phys. Chem. Lett.* **2015,** *6*, 4774–4785.
(40) Mao, L.; Tsai, H.; Nie, W.; Ma, L.; Im, J.; Stoumpos, C. C.; Malliakas, C. D.; Hao, F.; Wasielewski, M. R.; Mohite, A. D.; Kanatzidis, M. G. Role of Organic Counterion in Lead- and Tin-Based Two-Dimensional Semiconducting Iodide Perovskites and Application in Planar Solar Cells. *Chem. Mater.* **2016,** *28*, 7781-7792.

A new ABX_3-type hybrid organic-inorganic guanidnium hypophosphite perovskite [Gua][$Mg(H_2POO)_3$], which exhibits a second-order irreversible phase transition at about 291 K and reveals significant NTE effect along *b*-axis. In addition, the calculated band structure and density of states demonstrate that the Gua cations donate to the large direct bandgap.

Insert Table of Contents artwork here